

JGR Space Physics

RESEARCH ARTICLE

10.1029/2022JA030319

Key Points:

- Swarm encounters peaks of electron density at the dayside dip equator under zero magnetic declination, which is arguably an artifact
- The artifacts occur for all seasons and solar activity, and for both ascending/descending
- We suggest that the artifacts are associated with enhanced secondary electrons escape under favorable magnetic field configurations

Correspondence to:

H. Song,
hssong@kasi.re.kr

Citation:

Song, H., Park, J., Buchert, S., Jin, Y., Chao, C. K., Lee, J., & Yi, Y. (2022). A Small peak in the Swarm-Lp plasma density data at the dayside dip equator. *Journal of Geophysical Research: Space Physics*, 127, e2022JA030319. <https://doi.org/10.1029/2022JA030319>

Received 25 JAN 2022

Accepted 22 JUN 2022




Author Contributions:

Conceptualization: Jaeheung Park
Data curation: Stephan Buchert, Yaqi Jin
Formal analysis: Hosub Song
Funding acquisition: Jaejin Lee
Investigation: Hosub Song, Jaeheung Park, Stephan Buchert
Project Administration: Jaejin Lee
Software: Hosub Song
Validation: Jaeheung Park
Visualization: Hosub Song
Writing – original draft: Hosub Song
Writing – review & editing: Hosub Song, Jaeheung Park, Stephan Buchert, Yaqi Jin, Chi Kuang Chao, Jaejin Lee, Yu Yi

© 2022. The Authors.

This is an open access article under the terms of the [Creative Commons Attribution-NonCommercial-NoDerivs License](https://creativecommons.org/licenses/by/4.0/), which permits use and distribution in any medium, provided the original work is properly cited, the use is non-commercial and no modifications or adaptations are made.

A Small Peak in the Swarm-LP Plasma Density Data at the Dayside Dip Equator

Hosub Song^{1,2} , Jaeheung Park^{1,3} , Stephan Buchert⁴ , Yaqi Jin⁵ , Chi Kuang Chao⁶ , Jaejin Lee¹ , and Yu Yi² 

¹Space Science Division, Korea Astronomy and Space Science Institute (KASI), Daejeon, South Korea, ²Department of Astronomy, Space Science and Geology, Chungnam National University (CNU), Daejeon, South Korea, ³Department of Astronomy and Space Science, University of Science and Technology (UST), Daejeon, South Korea, ⁴Swedish Institute of Space Physics, Uppsala, Sweden, ⁵Department of Physics, University of Oslo, Oslo, Norway, ⁶Department of Space Science and Engineering, National Central University, Taoyuan, Taiwan

Abstract In this paper, we statistically investigate an artifact in Langmuir Probe (LP) observations of Swarm satellites. A small peak of electron density (N_e) is frequently found in the Swarm data around the dayside dip equator. On the contrary, they appear in neither the Total Electron Content data of the Swarm/Global Positioning System Receivers nor COSMIC-2 in-situ measurements at similar altitudes but with low orbit inclination. Arguably, this peak does not represent natural ionospheric irregularities but is likely to result from artifacts. The phenomena are found regardless of the season, solar activity, and the velocity direction of the satellite (ascending and descending). They predominantly occur when the magnetic declination is close to zero, that is, when the Swarm ram direction and the Earth's magnetic field are aligned under sunlight. Hence, we attribute the phenomenon to intensified secondary electrons escape when the geomagnetic field lines are normal to conducting surfaces that emit secondary electrons. Since the magnitude of the artifact is only a few percent of the large-scale background, it does not have a serious impact on the value of the Swarm/LP data in scientific research. Nevertheless, future efforts to determine the exact cause of the artifacts will contribute to improving the reliability and quality of plasma density and temperature measured by Swarm/LP.

Plain Language Summary In this paper, we statistically investigate artifacts found in Langmuir Probe (LP) observations of Swarm satellites and search for their possible causes. LP is an instrument that measures the density and temperature of charged particles (so-called “plasma”) around the satellite. Unexpectedly, small peaks of plasma density often occur around the dayside dip equator in the Swarm/LP data, while they are not at all observed in other similar equipment, such as Swarm Global Positioning System Receivers or COSMIC-2 satellites' ion probes at similar altitudes. For this reason, we deem this peak an artifact. This phenomenon occurs in all seasons, solar activity, and satellite movement directions. But, it predominantly appears when the ram direction of Swarm is nearly aligned with the Earth's magnetic field under sunlight. Hence, we consider that it originates from enhanced secondary electrons escape under a particular magnetic field configuration. The artifacts do not have a deleterious impact on scientific research because they are only a few percent of the background. However, efforts to determine the exact cause of artifacts are warranted for improving the reliability and quality of LP data.

1. Introduction

Plasma technologies play an essential role in our contemporary life, such as in food pasteurization, the disinfection of medical tools, and the manufacture of semiconductors. Accordingly, plasma diagnoses using various methods (e.g., Abdu et al., 1991; Lee et al., 2013; Takahashi et al., 1981) are becoming more and more important. Langmuir Probe (LP) was first designed by Langmuir in 1924 to diagnose gas discharge in laboratory chambers (Langmuir & Mott-Smith, 1924) and has been intensively used for observing ionosphere and magnetosphere in space (Marks, 2011). It applies a variable voltage (V) to a conducting probe surface, after which the electric current (I) collected by the probe is measured (Hoang et al., 2019; Marholm & Marchand, 2020; Oyama, 2015; Smirnov et al., 2021). The current-voltage (I–V) characteristics curve, which represents the relationship between the applied voltage, also called “bias,” and the measured current (Amatucci et al., 2001), is a key output from the probe. It should be noted that the spacecraft is subject to the sheath effect, which alters the properties of the plasma within the Debye length. Therefore, the mounting posts of LPs should provide enough spatial separation

between the probe and the spacecraft (Smirnov et al., 2021). In general, two approximations are used to express the electric current exchanged between the probe and the plasma: orbital motion limited and sheath area limited (Abe & Oyama, 2013; Langmuir & Mott-Smith, 1924). From the I–V curve, one can derive the temperature and density of thermal electrons. The temperature and density of ionospheric thermal plasma are important parameters for characterizing the overall ionosphere (Abe & Oyama, 2013), whose state can affect communication/navigation and the operation of satellites (Marks, 2011).

LPs come in a variety of shapes, and their data are processed by analytical or empirical expressions for plasma diagnoses. The probes are used in different operational modes, depending on what they are to measure (Marholm & Marchand., 2020). The LPs have been frequently installed on Low Earth Orbit (LEO) satellites for determining the basic characteristics of the space plasma (Abe & Oyama, 2013). The first in-situ measurement of electron temperature in the ionosphere was made by Langmuir in 1947 (Abe & Oyama, 2013; Oyama, 2015; Reifman & Dow, 1949). Even in recent decades, to name a few relevant missions, the Swedish micro-satellite Astrid-2 was launched on 10 December 1998, piggyback on a Cosmos-3M rocket, into a circular orbit at 1,000 km altitude with Langmuir Interferometer and Density instrument for Astrid-2 as a payload (Holback et al., 2001; Marklund et al., 2001). On 15 July 2000, the Challenging Minisatellite Payload (CHAMP) was launched to observe the Earth's gravity, magnetic field, neutral atmosphere, and ionosphere, the last of which were monitored with the Planar Langmuir Probe (PLP) (Cooke et al., 2003; Gorbunov & Kornbluh., 2003; Heise et al., 2002; Lee et al., 2011). On 29 June 2004, Detection of Electro-Magnetic Emissions Transmitted from Earthquake Regions (DEMETER) was launched and placed in a polar, circular, and quasi sun-synchronous orbit (10.30 and 22.30 in local time; LT) at an altitude of 710 km (Sarkar et al., 2007). DEMETER had a LP instrument, called “Instrument Sonde de Langmuir” (ISL) to map the bulk plasma parameters (primarily electron density and temperature) and to study their variations associated with earthquakes and other sources of perturbations (Kakinami et al., 2013; Lebreton et al., 2006). On 16 April 2008, Communications/Navigation Outage Forecasting System (C/NOFS) satellite developed by the Air Force Research Laboratory was launched into a low-inclination (13°) orbit with a perigee near 400 and an apogee near 850 km (Bilitza et al., 2012; Costa et al., 2014). Using its PLP, C/NOFS is capable of measuring in situ ion density within the low-latitude F-region (Dao et al., 2011). On 2 November 2009, the PROBA-2 spacecraft was launched from Plesetsk as a secondary passenger onboard a rocket launcher (Côté et al., 2011). PROBA-2 had the Dual Segmented LP (DSLPL) instrument to measure the density of space plasma and its variations, the electron temperature, and the satellite potential (Rochus et al., 2004). The DSLPL is of ISL heritage flown on the DEMETER mission (Gantois et al., 2006). On 22 November 2013, Swarm satellites were launched from the Plesetsk Cosmodrome, and a pair of LPs are carried by each spacecraft to measure electron density and temperature (Buchert et al., 2015; Knudsen et al., 2017).

Depending on the sign of the bias, the probe current depends on the flux of positively charged ions, at negative bias, or on the density of negative electrons, at positive bias, respectively. The analysis of the probe current can provide estimates of both the ion density N_i for known ion mass and the electron density N_e , in the different bias regimes, respectively (Ryu et al., 2017). Ion and electron densities can be different when electrons attach to molecular ions and/or dust particles (Morooka et al., 2018). In the Earth's F region ionosphere charging of dust and molecules is expected to be insignificant, and ion and electron densities are equal. The Swarm LP processing chain estimates the ion density in the negative bias regime. The estimate is then used as a reliable proxy for the electron density, and labeled “ N_e ” in the data product and this paper.

Despite the long heritage in space plasma research, the quality of the LP data still has some inherent issues. For example, LP operations are likely to be compromised when a satellite passes through solar terminators (Ivarsen et al., 2019; Yan et al., 2022). Also, the data can sometimes exhibit an anomaly that makes the electron density and temperature unstable (Jin et al., 2020). The electrode surfaces of LPs can also be oxidized, causing measurement glitches by distorting current-voltage (I–V) characteristics (Pyu et al., 1995; Samaniego et al., 2018). Furthermore, errors can appear due to contamination of probe surfaces (Fang et al., 2018; Oyama, 1976). The contamination leads to hysteresis in the I–V curve: that is, the curve takes different shapes depending on whether the applied voltage is swept upward or downward (Hirao & Oyama., 1971; Hirt et al., 2001; Jiang et al., 2020; Winkler et al., 2000). To overcome the interference of the contaminated layer in the LP measurement, Szuszczewicz and Holmes (1975) used a discrete pulse scan instead of a continuous triangular wave scan: this type of LP is called a “pulsed LP.” Oyama et al. (2012) studied the time interval of LP pulses and proposed the pulse on/off time ratio of 1/99 gives the same result as the uncontaminated probe characteristic curve. There can be another constraint

for LPs, in the case of a small satellite: a conducting area of the satellite body should be much larger than the conducting area of the probe. Since the electric potential applied to an LP has the reference point (i.e., electric ground) at the satellite body, the latter should be stably maintained to the space plasma potential. However, if the conducting area of the satellite is not hundreds of times larger than the conducting area of the probe, the LP operation can be significantly degraded (Lee et al., 2013).

To validate and recalibrate the LP measurements that can be subject to the inherent limitations as mentioned above, scientists usually compare the post-launch LP data with ground-based observations. McNamara et al. (2007) compared the PLP data of CHAMP with the ionosonde density profiles over Jicamarca, Peru. The electron temperature data of CHAMP was also validated by incoherent scatter radar data of Arecibo and Tromsø (EISCAT), and the mean relative deviation was reduced to less than 3% through calibration (Rother et al., 2010). Larson et al. (2021) compared the electron density measured by Swarm/LP with the Resolute Bay Incoherent Scatter Radar data. Such comparison and/or calibration studies contributed to scientific research by providing reliability and increasing the accuracy of satellite data (Lomidze et al., 2018).

In this paper, we statistically investigate a small peak of plasma density in Swarm/LP observations over daytime dip equatorial regions. Section 2 gives a brief description of the instruments and data sets. We also present a representative example and demonstrate how to estimate the intensity of those peaks for every Swarm pass. In Section 3, the dependence of their occurrence on solar zenith/azimuth angle, magnetic declination angle, seasonal, and the direction of satellite velocity (i.e., ascending and descending nodes) are analyzed. We additionally address whether the peak can be observed by other instruments and/or spacecraft. Finally, we discuss possible causes of the phenomenon in Section 4 and draw conclusions in Section 5.

2. Swarm Satellites

The Swarm mission operated by European Space Agency (ESA) consists of three satellites at an altitude of 520 km (Swarm-B) and 470 km (Swarm-A, C), each having a near-polar orbit (Schreiter et al., 2021). The inclination angles are about 88°, which means that the orbits are approximately aligned with the geographic meridian (Park et al., 2015). The prime purpose of the mission is to study the internal and external magnetic fields of the Earth and to observe the electric and plasma states of the ionosphere (Knudsen et al., 2017). The payloads on board are Vector Field Magnetometer, Absolute Scalar Magnetometer, Electric Field Instrument (EFI), GPS Receivers (GPSR), and Laser Retro-Reflectors (Gvishiani et al., 2016; Marchetti & Akhoondzadeh, 2018). In particular, the EFI consists of two Thermal Ion Imagers (TIIs) on a faceplate and two LPs below TIIs (Rehman et al., 2012; Singh et al., 2021). The LPs of Swarm measure electron density (N_e), electron temperature (T_e), and floating potential with a nominal time resolution of 2 Hz (Knudsen et al., 2017; Singh et al., 2021).

The GPSR onboard Swarm is a multi-channel receiver that receives up to eight GPS signals simultaneously at 1 Hz (Zakharenkova et al., 2019). The phase of GPS L1-L2 carriers is related to Total Electron Content (TEC), which is the integrated number of electrons along the path between each Swarm satellite and the GPS satellites (Dahle et al., 2017; Hong et al., 2017; Hussien et al., 2020; Lee et al., 2007; Schreiter et al., 2021). TEC can be used as a proxy of the in-situ plasma density (e.g., Noja et al., 2013, Figure 8). In this study, we use the LP and TEC data compiled into the Ionospheric Plasma Irregularities (IPD) product that has 1 Hz data rate (Jin et al., 2022).

The faceplate controls the entrance of ions into the TII instrument mechanically and also via a negative bias (Knudsen et al., 2017). The LP sets the faceplate bias and monitors its current. Thus another independent estimate of the ion density is obtained at 16 Hz resolution, similar to a PLP, but without the ability to sweep the bias and to measure T_e . The faceplate density estimate is available only when the TII is inactive (Aol et al., 2020).

In addition, FormoSat-7/COSMIC-2 satellite data is compared with Swarm satellite data. The COSMIC-2 satellites, which the National Space Organization/National Applied Research Laboratories (NSPO/NARL) in Taiwan and the National Oceanic and Atmospheric Administration (NOAA) in the United States collaborated on, were launched on 25 June 2019. The final destination altitude is about 550 km (Schreiner et al., 2020), which is similar to that of Swarm-Bravo (~520 km). These six COSMIC-2 satellites have Ion Velocity Meters (IVMs) that measure ion temperature, velocity, and density (Yue et al., 2014). An important difference between Swarm and COSMIC-2 is the orbit inclination: the former orbit is nearly aligned with the geographic meridian (orbit

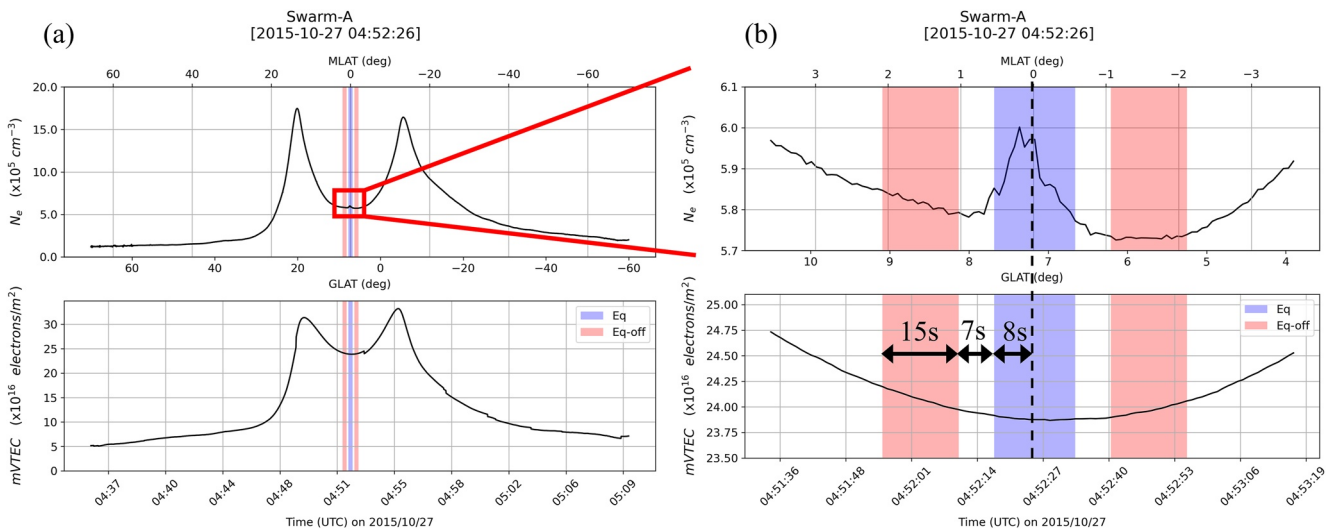


Figure 1. Electron density (N_e) and Total Electron Content (TEC) plots of Swarm-A. The top row has electron density as the y-axis, and the bottom graphs present TEC. Figure 1a shows electron density and TEC during an equator crossing, and Figure 1b is an enlarged graph around the magnetic equator. Panels in each column share the same Magnetic LATitude (MLAT), Geographic LATitude (GLAT), and Universal Time Coordinated (UTC) on the x-axis. Concerning the magnetic equator, we pick up three different regions for statistical analyses: a blue shadow (Eq) for ± 8 s, and two red shadows (Eq-off) for 15 s after having a buffer of 7 s. The N_e ratio is the ratio of the mean N_e values over the blue and red shadows. The N_e ratio is a proxy for the intensity of the equatorial peaks and will be used throughout the rest of this paper. If the N_e ratio is larger than unity, it means that the average value of N_e in the blue shadow is larger than in the red shadows, so we consider that an equatorial peak occurs.

inclination $\sim 88^\circ$) while that of the latter is much smaller (orbit inclination $\sim 24^\circ$). That is to say, the Swarm ram direction can sometimes be aligned with geomagnetic field lines at low latitudes. On the contrary, such alignment between spacecraft orbit and the magnetic field is inherently impossible for COSMIC-2. In this study, we use COSMIC-2 data obtained at altitudes at and below 550 km for comparison with Swarm observations.

The target phenomenon we are going to investigate in this paper is a small peak of electron density near the dayside dip equator, which is different from two giant off-equatorial peaks known as Equatorial Ionization Anomaly. Figure 1 is a representative example of this peak, which was observed by Swarm/LP on 27 October 2015. Figure 1a presents a wide view of a satellite pass, and Figure 1b is a zoom-up of the equatorial region. The upper row is the electron density and the lower row is the TEC profile. The x-axis represents Universal Time Coordinated (bottom axis), Geographic LATitude (middle axis), and Magnetic LATitude (top axis) along the Swarm orbit. Using Python's Apexy library, we find the dip equator and mark it with a black dashed line in Figure 1b. Regarding the black dashed line, the blue shadow (Eq) corresponds to ± 8 s on both sides, which represents the dip equatorial region hosting the small density peak. After a buffering interval of 7 s, two red shadows (Eq-off), each of which spans 15 s, are chosen: the red shadows signify off-equatorial ambient regions free from the equatorial peak. The ratio between the median electron density in the blue area (Eq) and that in the two red areas (Eq-off) is calculated (hereafter, called " N_e ratio") and deemed the strength of the equatorial peak. If the small peaks do not appear, the average electron density values of blue and red shades become similar, and thus the N_e ratio approaches 1. On the other hand, when a peak occurs in the blue shadow, the average value of N_e in the blue shadow is larger than in the red shadows, and the " N_e ratio" is greater than 1. For example, if the N_e ratio is 1.05, it means that the small peak size is 5%. Using this method implemented in Python, we analyze the entire LP (1 Hz) data and 16 Hz faceplate plasma data of Swarm satellites. Then, to investigate whether the equatorial peak is a true geophysical phenomenon or an artifact, we apply the same method to the Swarm GPS-TEC data and the plasma density data of COSMIC-2 satellites.

3. Result

Figure 2 shows the N_e ratio derived from Swarm observations from July 2014 to October 2021. The x-axis is the solar zenith angle (SZA) in degrees. When SZA is 0° , the Sun is on the zenith of Swarm, and when SZA is 180° , it is on the nadir. The SZA between 0° and 90° approximately corresponds to the dayside. The y-axis is the

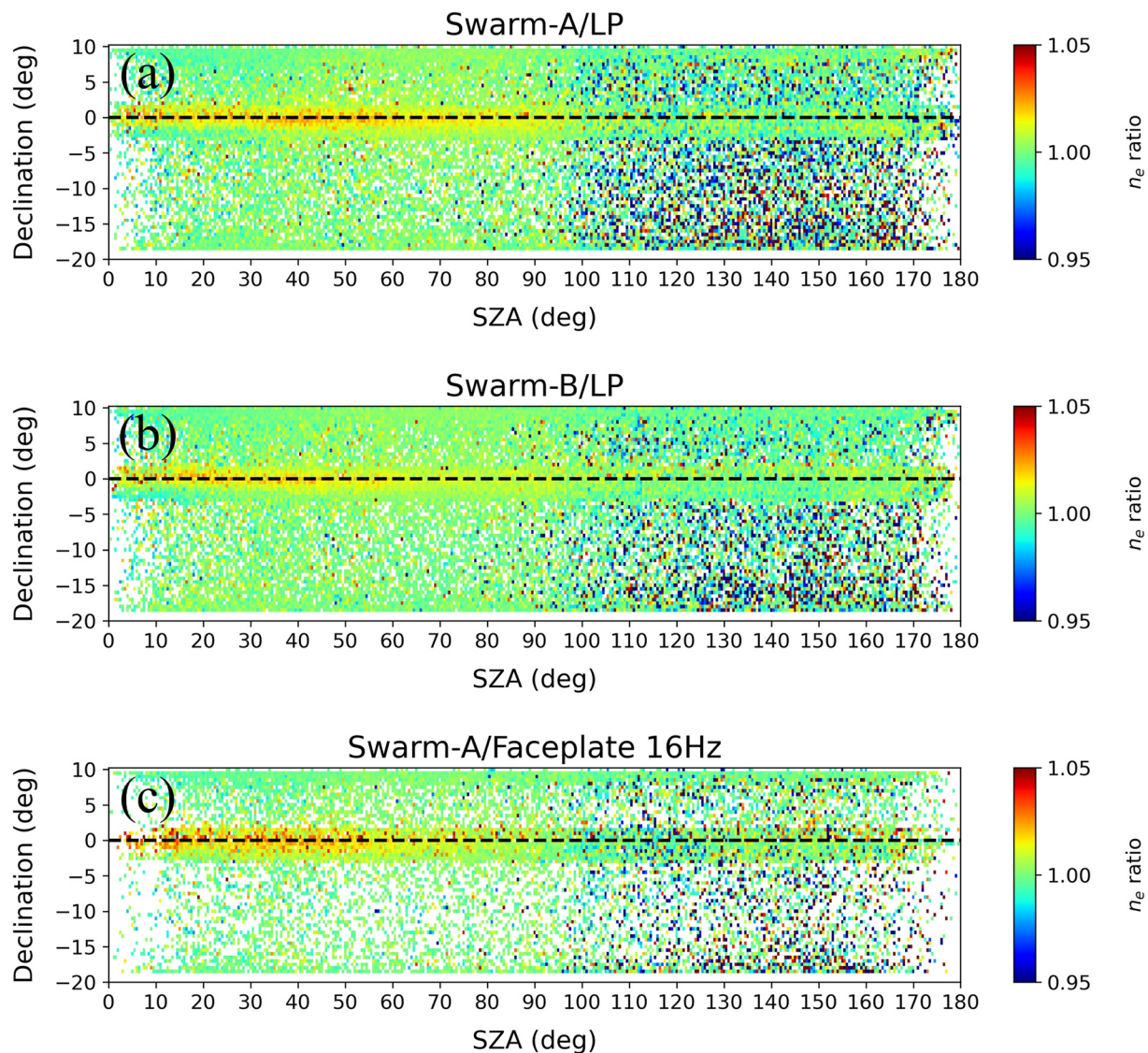


Figure 2. Color plots of electron density (N_e) ratio between equatorial and off-equatorial regions for Swarm Langmuir Probe (LP) and faceplate measurements. The horizontal axis is solar zenith angle, and the vertical axis is magnetic declination. Panel (a) presents the N_e ratio of Swarm-A/LP data, Panel (b) shows that of Swarm-B/LP data, and Panel (c) is about Swarm-A/Faceplate. A black dashed line is drawn to represent a magnetic declination of zero. Note that the color bar displays the N_e ratio in the range of 0.95–1.05.

magnetic declination (i.e., the angle between geomagnetic and geographic north directions) at the dip equator in degrees, and the color bar is the N_e ratio as described above. Whenever an equatorial peak as shown in Figure 1 occurs, the N_e ratio should be higher than unity and appear reddish in Figure 2. The black dashed line in each panel marks zero declination at the dip equator, meaning that the true North and the magnetic North coincide. As Swarm orbits are nearly aligned with the true North (orbit inclination angle $\sim 88^\circ$), the black dashed line of “zero-declination at the dip equator” signifies that Swarm ram direction is nearly parallel to geomagnetic field lines. The upper graph (a) is LP data for the Swarm-A satellite (altitude ~ 470 km), the middle graph (b) is those of the Swarm-B satellite (altitude ~ 520 km), and the lower graph (c) is 16 Hz Faceplate data of the Swarm-A satellite. In Figure 2, it is immediately clear that the high N_e ratio (reddish color) is concentrated to the dayside (SZA $< 90^\circ$) and zero declination (black dashed line). This trend is common for both Swarm-A (Figure 2a) and Swarm-B (Figure 2b) and also for both the LP measurements (Figure 2a) and 16 Hz faceplate data (Figure 2c).

Figure 3 displays the geographic distribution of strong equatorial peaks, for which the N_e ratio of Swarm-A/LP data is higher than 1.03. The x-axis of all panels shares the same longitude. The red symbols in the upper panel

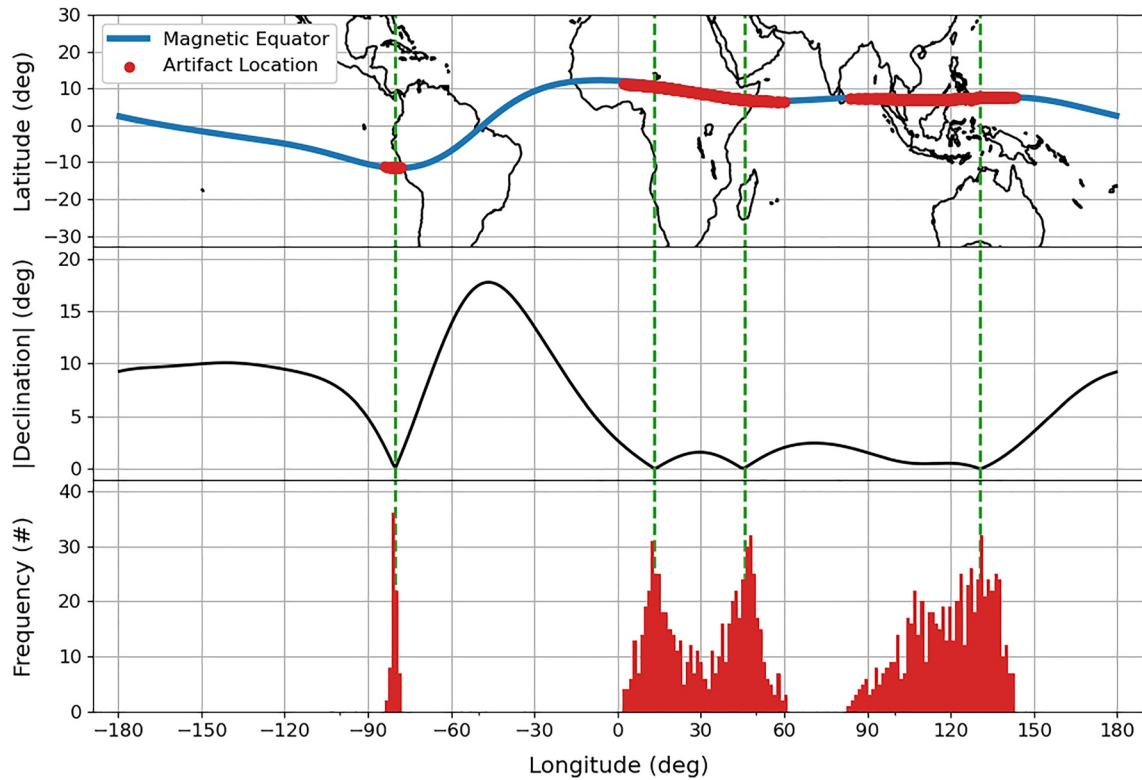


Figure 3. Distributions of strong equatorial peaks (N_e ratio > 1.03) in Swarm-A/LP data. The x-axis of all panels is geographic longitude. The top panel presents the location of the peaks with red symbols on the world map, and the blue line represents the dip equator. The middle panel is the absolute value of magnetic declination at the dip equator for each longitude. The bottom panel shows the frequency of the intense peaks as a histogram. Green vertical dashed lines indicate the longitudes at which the absolute value of the magnetic declination becomes zero in the middle panel. We can see that the equatorial peaks are absent in the longitudinal region of the large magnetic declination angle. The reason, which will be extensively discussed later in Section 4, is secondary electrons by the photoelectric effect, and the effect on the satellite varies depending on the magnetic declination.

show the place where the strong peaks (N_e ratio > 1.03) occurred on the world map: the x-axis is geographic longitude, and the y-axis is latitude. Also, the blue line represents the dip equator. The middle panel is the absolute value of magnetic declination at the dip equator, calculated using the `chaosmagpy` (<https://pypi.org/project/chaosmagpy/>) subroutine. The bottom panel represents the number of events satisfying the criterion (N_e ratio > 1.03). In the middle panel, the longitudes at which the absolute value of the magnetic declination becomes zero are indicated by green vertical dashed lines. Since the peaks of the histogram on the bottom panel are concentrated at the longitude points of the four green dashed lines, it is revealed that the strong equatorial peaks mainly occur in areas where the magnetic declination becomes zero. In summary, Figure 3 confirms Figure 2 in that the equatorial peaks predominantly occur where magnetic declination is zero around the dip equator: that is, where the geographic and magnetic North directions (as well as the Swarm ram directions) are nearly parallel.

We note that no previous studies ever reported on such small density peaks around the daytime dip equator that we are addressing. Considering the long history of LEO plasma measurements, it is highly possible that the peaks in Figures 1–3 are not truly natural phenomena, but artifacts. To support this conjecture, we applied the same analysis method to other independent data sets, whose results are shown in Figure 4: (a) Swarm-A GPS TEC and (b) plasma density measured by COSMIC-2. Figure 4a presents TEC data of Swarm-A, which are processed in the same way as for the LP data: the result is called “TEC ratio” hereafter. Note that TEC is expected to have a reasonable correlation with LP measurements (e.g., Noja et al., 2013, Figure 8). Figure 4b is the N_e ratio of COSMIC-2, which has similar altitudes as that of Swarm-B, but a much smaller orbit inclination ($\sim 24^\circ$) than Swarm ($\sim 88^\circ$). As COSMIC-2 satellites have different orbit inclination from those of Swarm, the N_e ratio is calculated with slightly different window lengths: 8, 7, and 15 s windows in Figure 1 become 19.669, 17.210, and 36.879 s by considering a factor of $\sin(24^\circ)$ for COSMIC-2. In this way, the latitude range used for deriving the N_e ratio would be comparable between Swarm and COSMIC-2. In Figure 4, neither panel shows conspicuous red

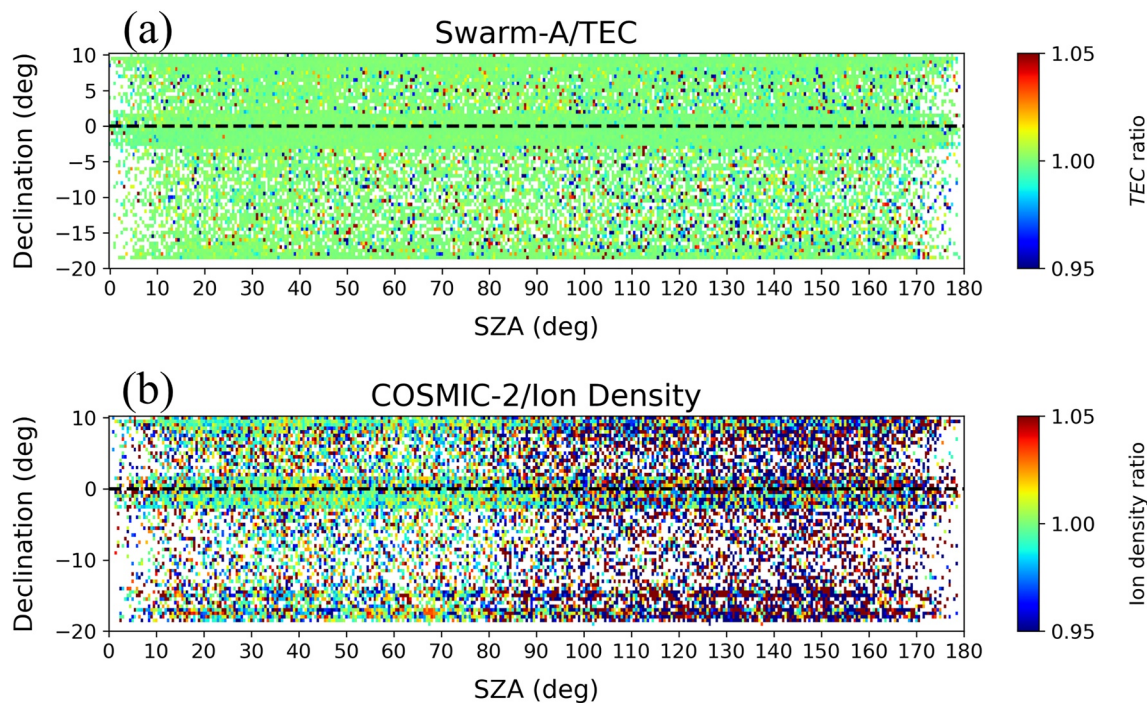


Figure 4. Similar to Figure 2, but for (a) TEC ratio from Swarm-A and (b) N_e ratio from COSMIC-2.

pixels near the black dashed line. Therefore, the peaks observed by Swarm/LP near the daytime dip equator (e.g., Figures 1 and 2) are considered “artifacts,” because they occur only in electron density data measured by Swarm/LP and Faceplate, and do not appear in Swarm/TEC data or COSMIC-2/ion density data.

Now we elucidate what background conditions are favorable for the occurrence of the daytime equatorial N_e peaks. Figure 5 is similar to Figure 2a, but sub-categorized by seasons (Equinoxes: Mar., Apr., Sep., Oct.; June solstice: May–August; December solstice: November–February) and solar activity levels. The three panels on the left are for the solar maximum before 1 January 2018, and the three on the right are for the solar minimum after 1 January 2018. Also, the graphs at the top are the northern spring and autumn (equinox), the middle graphs are the northern summer (June solstice), and the bottom graphs are the northern winter (December solstice) season. The black horizontal dashed line indicates zero declination, and the reddish area corresponding to the N_e ratio

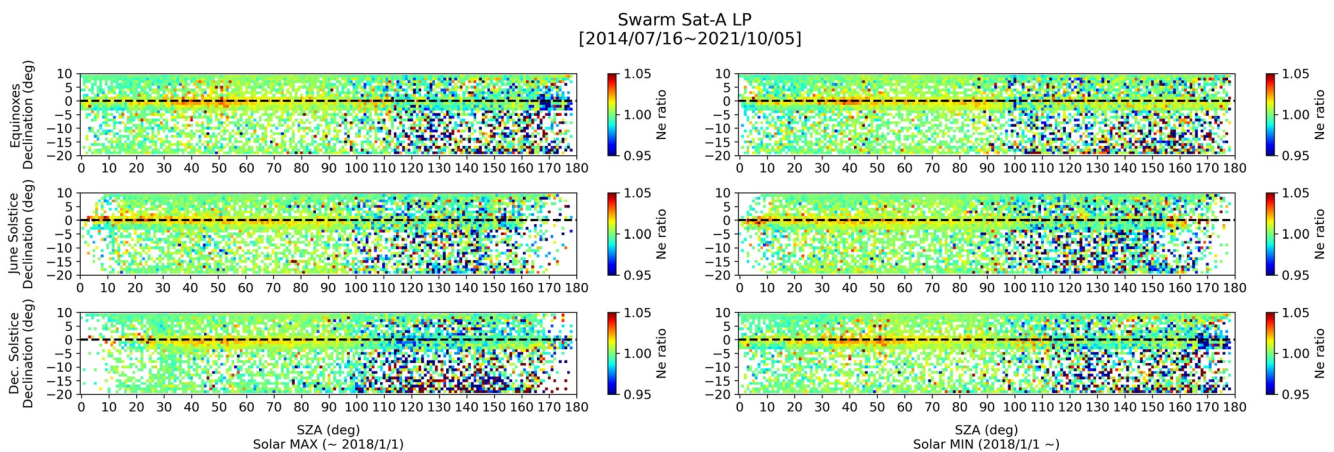


Figure 5. Color plots of N_e ratio for different seasons and solar cycle phases. The left column panels are solar maximum before 2018/1/1, and the right column panels are solar minimum after 2018/1/1. The top row corresponds to Equinoxes, the middle row to June Solstice, and the bottom row to December Solstice. The x-axis is solar zenith angle (SZA), the y-axis is magnetic declination, and the color palette is the N_e ratio.

of data = 35,522 ($|\text{DEC}| < 3$)
[2014/07/16~2021/10/05]

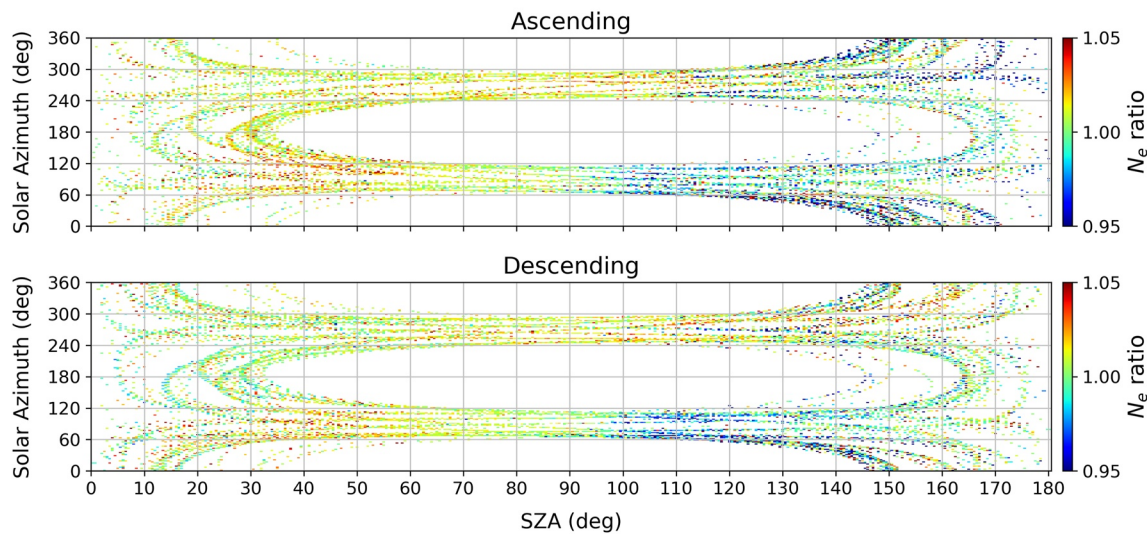


Figure 6. Color plots of N_e ratio as a function of solar zenith angle (SZA) and solar azimuth angle. The top panel is the ascending direction in which the satellite moves northward, and the bottom panel is the descending direction in which it moves southward. The x-axis is SZA, and the y-axis is the solar azimuth angle at the dip equator. The data used are from Swarm-A/LP for all periods, but only the data points for which the absolute value of magnetic declination is less than 3° are taken into account.

greater than 1 is concentrated around the dashed line when the SZA is less than 90° . Figure 5 demonstrates that the daytime equatorial peaks occur in the LP data of Swarm-A in all solar cycle phases and seasons.

Similarly, we analyze the association of the N_e ratio with the solar azimuth as shown in Figure 6. To focus on strong equatorial peaks, only the data points for which the absolute value of magnetic declination is less than 3° are used (e.g., see Figure 3). The x-axis of Figure 6 is SZA, the y-axis is the solar azimuth angle (0° when the Sun is northward of Swarm, and 90° when the Sun is to the east), and the color palette represents the N_e ratio. As the Sun is located around 12 LT, a solar azimuth angle of $0^\circ \sim 180^\circ$ on the dayside (SZA $< 90^\circ$) signifies that Swarm is in the prenoon LT. Similarly, a solar azimuth angle of $180^\circ \sim 360^\circ$ on the dayside (SZA $< 90^\circ$) signifies that Swarm is in the postnoon LT. The top panel represents when the satellite travels northward and passes through the ascending node. Similarly, the bottom panel is when the satellite passes through the descending node moving southward. We cannot find a conspicuous preference for a certain solar azimuth angle. When we focus on the dayside (SZA $< 90^\circ$), the N_e ratio seems to be slightly higher when the Sun is located to the East of Swarm (i.e., Swarm in the prenoon sector; solar azimuth $< 180^\circ$) than otherwise (i.e., Swarm in the postnoon sector; azimuth $> 180^\circ$) for both Ascending and Descending nodes. In other words, Figure 6 demonstrates that the dayside equatorial peak is slightly more conspicuous before noon than in the afternoon.

4. Discussion

4.1. Possible Generation Mechanisms

In the previous Section, we have shown that small density peaks are frequently found in the Swarm/LP and faceplate N_e data. As no previous study reported similar geophysical phenomena, and as the peaks are absent in Swarm/TEC data and COSMIC-2 in-situ observations at similar altitudes, we deem the dayside equatorial peak as an artifact. In this Section, we discuss possible mechanisms that may have led to the peaks. Since this phenomenon is related to sunlight and zero magnetic declination (see Figures 2 and 3), we suggest that it originates from secondary electrons escape facilitated under certain magnetic field configurations by the photoelectric effect. As depicted in Figure 7, under the influence of the geomagnetic field, secondary electrons

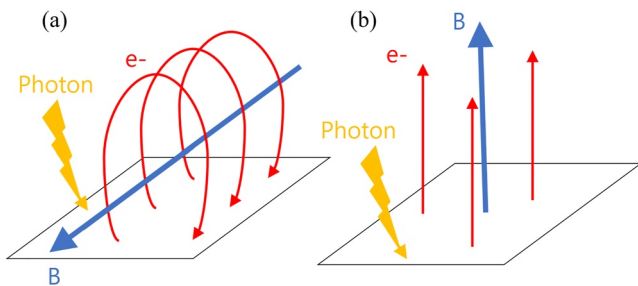


Figure 7. The conceptual diagram of the trajectory (red) of (a) returning electrons and (b) escaping electrons generated by photoelectric effects (yellow) in a magnetic field (blue).

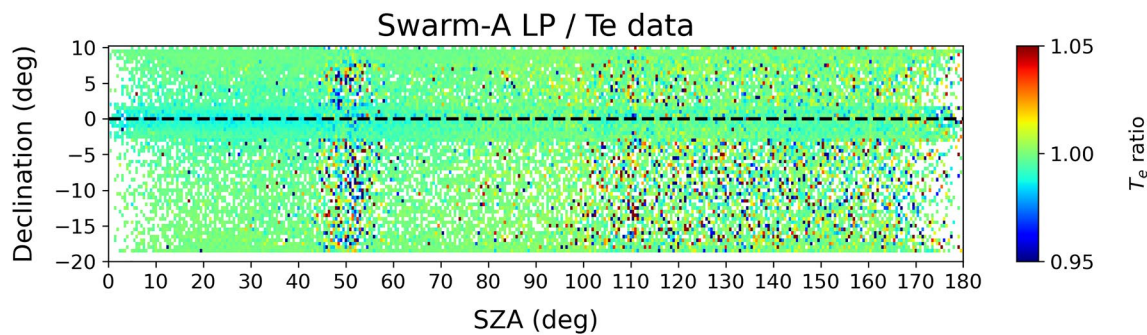


Figure 8. Similar to Figure 2, but showing a color plot of electron temperature (T_e) ratio from Swarm-A/LP.

generated by sunlight are likely to return to the surface which they came from (Figure 7a) due to the gyromotion. In this case, the secondary electrons can generate no net current (Wang et al., 2014). For example, if secondary electrons originate from the LP surface and immediately return to it, they would hardly induce sensible current to LP electronics. However, the escape of secondary electrons depends on the direction of the magnetic field concerning the emitting surface (Costin, 2021). The escape is facilitated when the magnetic field is perpendicular to the surface of the satellite (Figure 7b; also Laulainen et al., 2016). When the magnetic field is normal to the surface, the amount of secondary electrons escaping from the surface (e.g., LP surface) is more than doubled (Anashin et al., 2001). On the contrary, electrons are returned when the satellite's surface is parallel to the magnetic field (i.e., grazing magnetic fields), such as in Figure 7a.

We remind the readers that dayside equatorial peaks in Figure 1 frequently occur under the condition of zero declination at the dip equator. The condition (at the dip equator and where the declination is near zero) means that the Swarm's ram direction is nearly parallel to the geomagnetic field lines (or the ram surface is normal to the magnetic field, which corresponds to Figure 7b). For negative bias as is used for Swarm/LP, escaping secondary electrons would produce a stronger ion current with a correspondingly higher ion density estimate (labeled " N_e "). This effect is absent if the secondary electrons return to the probe due to the magnetic gyro motion at non-zero declination (see Figure 7a). The thermal electron gyroradius is about 2–3 cm for typical conditions at equator crossings by Swarm. For secondary electrons, the gyroradius becomes larger. Assuming typical values for the geomagnetic field strength (40,000 nT) and secondary electron energy (2 eV), the gyroradius of secondary electrons is ~ 10 cm. This would allow secondary electrons to return to the faceplate, with a dimension of about 20 cm. The LP diameter is 0.8 cm, smaller than the gyroradius, which might prevent secondary electrons from returning to the probe. However, a small density enhancement is observed for estimates with both instruments, that is, the faceplate and the LP. Possibly, lower-energy secondary electrons (e.g., 0.1 eV), if any, may fit better in situations described in Figure 7 because they would have gyroradii of a few centimeters. The explanation of the escaping and the non-escaping secondary electrons should in the future be investigated in more detail.

The dependence of the daytime N_e ratio on solar azimuth (Figure 6) can also be put into the same context. When Swarm is in a prenoon sector (SZA $< 90^\circ$ and solar azimuth $< 180^\circ$), the ambient electron density is smaller than in the afternoon (Lomidze et al., 2018, Figure 5). As the ambient ionosphere gets more tenuous, relative effects of secondary electrons (in comparison to those of the ambient thermal plasma) on Swarm/LP would become stronger. That may explain why the daytime N_e ratio in Figure 6 is slightly stronger before noon (solar azimuth $< 180^\circ$) than in the afternoon (solar azimuth $> 180^\circ$).

For COSMIC-2, whose orbit inclination is only 24° , its ram direction can in no way be aligned with the geomagnetic field. This difference can explain the absence of such peaks in the COSMIC-2/IVM data. As the Swarm GPS antenna looks upward on top of the Swarm spacecraft, the TEC data can be free from the effect of this secondary electron because Swarm/LP is placed at the bottom of the satellite: that is, the GPS antenna and LP are separated well by the large spacecraft body. Therefore, we suggest that the daytime equatorial peaks observed by Swarm/LP, which are very likely to be artifacts, are related to enhanced secondary electrons escape from the LP surface when the Swarm ram direction is aligned with the geomagnetic field.

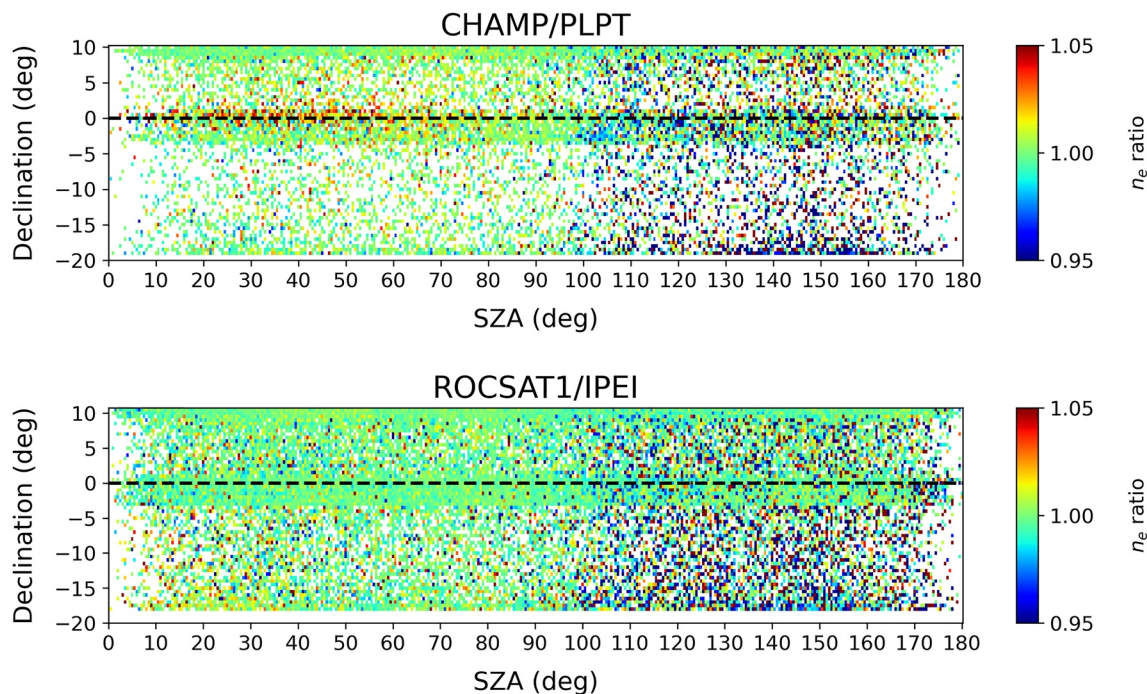


Figure 9. Color plots of electron density (N_e) ratio between equatorial and off-equatorial regions for (a) Challenging Minisatellite Payload (CHAMP) and (b) ROCSAT-1. The x-axis is SZA, and the y-axis is magnetic declination. A black dashed line is drawn to represent a magnetic declination of zero. Note that the color bar displays the N_e ratio in the range of 0.95–1.05. The top panel is about CHAMP having a large inclination angle of 87.18° and shows that the high N_e ratio (reddish color) is concentrated to the dayside ($\text{SZA} < 90^\circ$) and zero declination (black dashed line) like in Figure 2 about Swarm. The bottom panel is about ROCSAT-1 having a small inclination angle of 35° , and does not display the reddish area on dayside ($\text{SZA} < 90^\circ$) and zero declination (black dashed line) like for COSMIC-2.

4.2. Effects on Electron Temperature Measurements

For completeness, we apply the same method as demonstrated in Figure 1 to electron temperature measured by Swarm/LP: hereafter “ T_e ratio.” Figure 8 is similar to Figure 2, but presents the T_e ratio of Swarm-A/LP. Note that previous studies found a few quality issues in electron temperature measured by Swarm/LP. Caution was urged for Swarm/LP electron temperature data (a) when SZA is about 50° (Jin et al., 2020; Figures S2-S3) and (b) at nightside regions hosting plasma irregularities (Rodríguez-Zuluaga et al., 2019). These two well-known artifacts are also visible in Figure 8: (a) a noisy vertical band around $\text{SZA} \sim 50^\circ$ and (b) overall complex behavior of T_e ratio at night ($\text{SZA} > 90^\circ$). Besides these noisy regions, when the declination is 0° and $\text{SZA} < 90^\circ$, a blue area having a ratio lower than 1 appears. That is, the equatorial density peak in Figure 2 is accompanied by the (apparent) local decrease of electron temperature. As the former (N_e ratio enhancement) is likely to be artifacts as mentioned before, so is the latter (concomitant electron temperature decrease). We should not misinterpret this temperature decrease as a natural phenomenon, for example, as a geophysical anti-correlation between ionospheric density and temperature reported in past studies (Kakinami et al., 2011; Su et al., 2015; Yang et al., 2020). Anyhow, both the density and temperature perturbations we address in this study have small magnitudes of a few percent (see the color bars in Figures 2 and 8), the existence of these artifacts would not seriously compromise the usefulness of Swarm/LP data for scientific research. Just, one needs to be careful when trying to find natural plasma irregularities in the dayside low-latitude ionosphere (e.g., Abdu et al., 1988; Huang et al., 2013; Kil et al., 2019) using Swarm data.

4.3. Further Supports From Observations During Solar Cycle 23

Despite the evidence given above, one may still suspect that the equatorial peaks represent a natural phenomenon similar to what was reported at low latitudes by Oya et al. (1991) and Shinbori et al. (2007). To give further support to our arguments that the peaks be artifacts, we add two more satellites to our analyses. Figure 9 is similar

to Figure 4, but for (a) (CHAMP, high-inclination satellite) and (b) Republic of China Satellite 1 (ROCSAT-1, low-inclination satellite). Both spacecraft measured in situ ion density during Solar Cycle 23. CHAMP had 87.18° of inclination (i.e., like Swarm), and the mission period was from 2000 to 2010 (Xiong et al., 2013). The PLP onboard CHAMP is similar to Swarm/LP in that both derive plasma density from the ion currents in the ion saturation regime (e.g., Knudsen et al., 2017; McNamara et al., 2007), where negatively biased probes collect the ions while repelling ionospheric and/or secondary electrons. On the contrary, traditional LPs mostly extracted plasma density in the “electron” saturation regime (e.g., Lee et al., 2013; Oyama, 2015), in which electrons are collected toward the probe surface. ROCSAT-1 (also known as Formosat-1) had 35° of inclination (i.e., like COSMIC-2), and the mission period was from 1999 to 2004. The Ionospheric Plasma and Electrodynamics Instrument (IPEI) onboard ROCSAT-1 belongs to the same family of ion probes as that of COSMIC-2/IVM. To sum up, CHAMP/PLP, Swarm/LP, ROCSAT-1/IPEI, and COSMIC-2/IVM all derive plasma density from collected ion currents, with the former two on near-polar (inclination angle ~90°) orbits and the latter two on low-inclination orbits.

As was the case for Swarm, the high inclination of the CHAMP orbit enables alignment between the ram direction and the geomagnetic field wherever the declination angle approaches zero at the dip equator. In Figure 9a, CHAMP observations clearly reveal the equatorial peak. On the other hand, ROCSAT-1 with a low inclination angle cannot be aligned with the geomagnetic field at all, and the equatorial peak does not appear in Figure 9b. Overall, the CHAMP and ROCSAT-1 results in Solar Cycle 23 respectively reproduce those of Swarm and COSMIC-2 in Solar Cycle 24–25. Observations by all the four satellites spanning two solar cycles can be summarized in the following one sentence: *plasma density estimated from ion current exhibits the equatorial peak when the spacecraft flies nearly along the geomagnetic field*. As mentioned in a previous section, the equatorial peaks' absence in COSMIC-2/IVM and presence in Swarm/LP, while both measured ion currents at similar altitudes, evidence that the equatorial peaks are artifacts. In this subsection, we have demonstrated that the equatorial peaks are similarly absent in ROCSAT-1/IPEI data while present in CHAMP observations, despite their overlapping observation periods. It corroborates the argument that the equatorial peaks are not geophysical.

In addition to the contrast in the orbit inclination angles, we note another small difference that distinguishes COSMIC-2/IVM and ROCSAT-1/IPEI from Swarm/LP and CHAMP/PLP. The latter group (Swarm/LP and CHAMP/PLP) has current collectors directly exposed to the space plasma environment, so that secondary electrons can freely escape under favorable magnetic field geometry. However, for the former group (COSMIC-2/IVM and ROCSAT-1/IPEI), the current collectors are protected by electrostatic grids with significant negative bias (called “suppressor grid”): see Chao & Su. (2020). The grid can additionally hinder secondary electron escape and can contribute to the absence of the equatorial peaks in COSMIC-2/IVM and ROCSAT-1/IPEI data. Quantifying the relative importance of the geomagnetic field effect and grid effect may be an interesting topic for future studies.

5. Conclusions

We analyze small N_e peaks that are frequently found in Swarm/LP and faceplate data near the dayside dip equator. This phenomenon appears regardless of the season, solar activity, and velocity direction (ascending/descending) of the satellite. The absence of similar structures in Swarm/TEC and COSMIC-2/IVM data, as well as the absence of relevant reports in previous studies, implies that it is arguably an artifact. This explanation is further corroborated by CHAMP and ROCSAT-1 observations during the preceding solar cycle (Solar Cycle 23), which exhibited similar inter-spacecraft discrepancy to that between Swarm and COSMIC-2. The equatorial N_e peaks in Swarm (and CHAMP) data predominantly occur when the magnetic declination is zero at the dip equator, that is, when the Swarm's (and CHAMP's) ram direction and the Earth's magnetic field are approximately aligned under sunlight. We suggest that the peak reflects enhanced secondary electrons escape when the geomagnetic field becomes normal to the Swarm's (and CHAMP's) ram surface. The secondary electrons currents can impact LP observation results: the secondary electrons entering and exiting the conductor can be misinterpreted by LPs as natural currents of the thermal plasma. Though the artifacts are small in magnitude (a few percent of the ambient), our study can contribute to further improving the reliability and quality of LP data in the future.

Data Availability Statement

The N_e , T_e , and TEC data of Swarm can be accessed from the official Swarm website of ESA (https://swarm-diss.eo.esa.int/#swarm%2FLevel2daily%2FLatest_baselines%2FIPD%2FIRR), and directory is Home-Level2daily-Latest_baselines-IPD-IRR data. Swarm Faceplate 16 Hz data is from the same Swarm website, and the directory is Home-Advanced-Plasma_Data-16_Hz_Faceplate_plasma_density. Ion density data of COSMIC-2 can be obtained through the COSMIC-2 data website (<https://data.cosmic.ucar.edu/gnss-ro/cosmic2/postProc/level2/>).

Acknowledgments

This research was supported by the Korea Astronomy and Space Science Institute under the R&D program (Project No. 2022-1-850-08) supervised by the Ministry of Science and ICT. JP was supported by the National Research Council of Science & Technology (NST) grant by the Korea government (MSIT; No. CPS21161-120).

References

- Abdu, M. A., Muralikrishna, P., Batista, I. S., & Chaves, A. H. P. (1988). On the rocket-induced wave disturbances in the daytime equatorial ionosphere. *Journal of Geophysical Research*, *93*(A4), 2758–2760. <https://doi.org/10.1029/JA093iA04p02758>
- Abdu, M. A., Muralikrishna, P., Batista, I. S., & Sobral, J. H. A. (1991). Rocket observation of equatorial plasma bubbles over Natal, Brazil, using a high-frequency capacitance probe. *Journal of Geophysical Research*, *96*(A5), 7689–7695. <https://doi.org/10.1029/90JA02384>
- Abe, T., & Oyama, K. (2013). *Langmuir probe* (pp. 63–75). An Introduction to Space Instrumentation. <https://doi.org/10.5047/aisi.010>
- Amatucci, W. E., Schuck, P. W., Walker, D. N., Kintner, P. M., Powell, S., Holback, B., & Leonhardt, D. (2001). Contamination-free sounding rocket Langmuir probe. *Review of Scientific Instruments*, *72*(4), 2052–2057. <https://doi.org/10.1063/1.1357234>
- Anashin, V. V., Collins, I. R., Dostovalov, R. V., Fedorov, N. V., Gröbner, O., Krasnov, A. A., et al. (2001). Magnetic and electric field effects on the photoelectron emission from prototype LHC beam screen material. *Vacuum*, *60*(1–2), 255–260. [https://doi.org/10.1016/S0042-207X\(00\)00392-4](https://doi.org/10.1016/S0042-207X(00)00392-4)
- Aol, S., Buchert, S., & Jurua, E. (2020). Traits of sub-kilometre F-region irregularities as seen with the Swarm satellites. *Annales Geophysicae*, *38*(1), 243–261. <https://doi.org/10.5194/angeo-38-243-2020>
- Bilitza, D., Brown, S. A., Wang, M. Y., Souza, J. R., & Roddy, P. A. (2012). Measurements and IRI model predictions during the recent solar minimum. *Journal of Atmospheric and Solar-Terrestrial Physics*, *86*, 99–106. <https://doi.org/10.1016/j.jastp.2012.06.010>
- Buchert, S., Zangerl, F., Sust, M., André, M., Eriksson, A., Wahlund, J. E., & Opgenoorth, H. (2015). Swarm observations of equatorial electron densities and topside GPS track losses. *Geophysical Research Letters*, *42*(7), 2088–2092. <https://doi.org/10.1002/2015GL063121>
- Chao, C. K., & Su, S.-Y. (2020). Charged particle motion inside the retarding potential analyzer. *Physics of Plasmas*, *7*(1), 101–107. <https://doi.org/10.1063/1.873817>
- Cooke, D. L., Roth, C., Luehr, H., & Jakowski, N. (2003). In situ plasma observation at 400 km on the CHAMP satellite. In *EGS-AGU-EUG joint assembly*. 13004.
- Costa, E., Roddy, P. A., & Ballenthin, J. O. (2014). Statistical analysis of C/NOFS planar Langmuir probe data. *Annales Geophysicae*, *32*(7), 773–791. <https://doi.org/10.5194/angeo-32-773-2014>
- Costin, C. (2021). Secondary electron emission under magnetic constraint: From Monte Carlo simulations to analytical solution. *Scientific Reports*, *11*(1), 1–11. <https://doi.org/10.1038/s41598-021-81345-x>
- Côté, J., Kron, A., De Lafontaine, J., Naudet, J., & Santandrea, S. (2011). PROBA-2 attitude and orbit control system: In-flight results of innovative GNC functions. *IFAC Proceedings Volumes*, *44*(1), 721–726. <https://doi.org/10.3182/20110828-6-IT-1002.03163>
- Dahle, C., Arnold, D., & Jäggi, A. (2017). Impact of tracking loop settings of the Swarm GPS receiver on gravity field recovery. *Advances in Space Research*, *59*(12), 2843–2854. <https://doi.org/10.1016/j.asr.2017.03.003>
- Dao, E., Kelley, M. C., Roddy, P., Retterer, J., Ballenthin, J. O., de La Beaujardiere, O., & Su, Y.-J. (2011). Longitudinal and seasonal dependence of nighttime equatorial plasma density irregularities during solar minimum detected on the C/NOFS satellite. *Geophysical Research Letters*, *38*(10). <https://doi.org/10.1029/2011gl047046>
- Fang, H. K., Chen, W. H., Chen, A. B., & Oyama, K. I. (2018). The effect of surface contamination of tiny satellite on DC probe ionosphere measurement. *AIP Advances*, *8*(10), 105220. <https://doi.org/10.1063/1.5052489>
- Gantois, K., Teston, F., Montenbruck, O., Vuilleumier, P., Braembussche, P. V. D., & Markgraf, M. (2006). *PROBA-2: Mission and new technologies overview*. European Space Agency, (Special Publication) ESA SP. 625 SP(September).
- Gorbunov, M. E., & Kornbluh, L. (2003). Analysis and validation of Challenging Minisatellite Payload (CHAMP) radio occultation data. *Journal of Geophysical Research*, *108*, 4584. <https://doi.org/10.1029/2002jd003175>
- Gvishiani, A., Soloviev, A., Krasnoperov, R., & Lukianova, R. (2016). Automated hardware and software system for monitoring the Earth's magnetic environment. *Data Science Journal*, *15*, 1–24. <https://doi.org/10.5334/dsj-2016-018>
- Heise, S., Jakowski, N., Wehrenpennig, A., Reigber, C., & Lühr, H. (2002). Sounding of the topside ionosphere/plasmasphere based on GPS measurements from CHAMP: Initial results. *Geophysical Research Letters*, *29*, 2–5. <https://doi.org/10.1029/2002GL014738>
- Hirao, K., & Oyama, K. (1971). Electron temperature observed with the Langmuir Probe and electron temperature Probe. *Journal of Geomagnetism and Geoelectricity*, *23*(2), 161–167. <https://doi.org/10.5636/jgg.23.161>
- Hirt, M., Steigies, C. T., & Piel, A. (2001). Plasma diagnostics with Langmuir probes in the equatorial ionosphere: II. Evaluation of DEOS flight F06. *Journal of Physics D: Applied Physics*, *34*(17), 2650–2657. <https://doi.org/10.1088/0022-3727/34/17/312>
- Hoang, H., Røed, K., Bekkeng, T. A., Moen, J. I., Clausen, L. B. N., Trondsen, E., et al. (2019). The multi-needle Langmuir Probe instrument for QB50 mission: Case studies of Ex-Alta 1 and Hoopoe satellites. *Space Science Reviews*, *215*(2), 21. <https://doi.org/10.1007/s11214-019-0586-x>
- Holback, B., Jacksén, Á., Åhlén, L., Jansson, S. E., Eriksson, A. I., Wahlund, J. E., et al. (2001). LINDA - the Astrid-2 Langmuir probe instrument. *Annales Geophysicae*, *19*(6), 601–610. <https://doi.org/10.5194/angeo-19-601-2001>
- Hong, J., Kim, Y. H., Chung, J. K., Ssessanga, N., & Kwak, Y. S. (2017). Tomography reconstruction of ionospheric electron density with empirical orthonormal functions using Korea GNSS network. *Journal of Astronomy and Space Sciences*, *34*(1), 7–17. <https://doi.org/10.5140/JASS.2017.34.1.7>
- Huang, C.-S., de La Beaujardiere, O., Roddy, P. A., Hunton, D. E., Ballenthin, J. O., & Hairston, M. R. (2013). Long-lasting daytime equatorial plasma bubbles observed by the C/NOFS satellite. *Journal of Geophysical Research: Space Physics*, *118*, 2398–2408. <https://doi.org/10.1002/jgra.50252>
- Hussien, F., Ghamry, E., Fathy, A., & Mahrous, S. (2020). Swarm satellite observations of the 21 August 2017 solar Eclipse. *Journal of Astronomy and Space Sciences*, *37*(1), 29–34. <https://doi.org/10.5140/JASS.2020.37.1.29>

- Ivarsen, M. F., Hoang, H., Yang, L., Clausen, L. B. N., Spicher, A., Jin, Y., et al. (2019). Multineedle Langmuir Probe operation and Acute Probe current susceptibility to spacecraft potential. *IEEE Transactions on Plasma Science*, 47(8), 3816–3823. <https://doi.org/10.1109/TPS.2019.2906377>
- Jiang, S. B., Yeh, T. L., Liu, J. Y., Chao, C. K., Chang, L. C., Chen, L. W., et al. (2020). New algorithms to estimate electron temperature and electron density with contaminated DC Langmuir probe onboard CubeSat. *Advances in Space Research*, 66(1), 148–161. <https://doi.org/10.1016/j.asr.2019.11.025>
- Jin, Y., Kotova, D., Xiong, C., Brask, S., Clausen, L. B. N., Kervalishvili, G., et al. (2022). Ionospheric Plasma Irregularities - IPIR - data product based on data from the Swarm satellites. *Journal of Geophysical Research: Space Physics*, 127, e2021JA030183. <https://doi.org/10.1029/2021JA030183>
- Jin, Y., Xiong, C., Clausen, L., Spicher, A., Kotova, D., Brask, S., et al. (2020). Ionospheric plasma irregularities based on in situ measurements from the Swarm satellites. *Journal of Geophysical Research: Space Physics*, 125, 1–17. <https://doi.org/10.1029/2020JA028103>
- Kakinami, Y., Kamogawa, M., Onishi, T., Mochizuki, K., Lebreton, J. P., Watanabe, S., et al. (2013). Validation of electron density and temperature observed by DEMETER. *Advances in Space Research*, 52(7), 1267–1273. <https://doi.org/10.1016/j.asr.2013.07.003>
- Kakinami, Y., Watanabe, S., Liu, J. Y., & Balan, N. (2011). Correlation between electron density and temperature in the topside ionosphere. *Journal of Geophysical Research*, 116, A12331. <https://doi.org/10.1029/2011JA016905>
- Kil, H., Paxton, L. J., Lee, W. K., & Jee, G. (2019). Daytime evolution of equatorial plasma bubbles observed by the first Republic of China satellite. *Geophysical Research Letters*, 46(10), 5021–5027. <https://doi.org/10.1029/2019GL082903>
- Knudsen, D. J., Burchill, J. K., Buchert, S. C., Eriksson, A. I., Gill, R., Wahlund, J. E., et al. (2017). Thermal ion imagers and Langmuir probes in the Swarm electric field instruments. *Journal of Geophysical Research: Space Physics*, 122, 2655–2673. <https://doi.org/10.1002/2016JA022571>
- Langmuir, I., & Mott-Smith, H. (1924). Studies of electric discharges in gases at low pressures. *General Electric Review*, 27(12), 810.
- Larson, B., Koustov, A. V., Kouznetsov, A. F., Lomidze, L., Gillies, R. G., & Reimer, A. S. (2021). A comparison of the topside electron density measured by the Swarm satellites and incoherent scatter radars over Resolute Bay, Canada. *Radio Science*, 56(11), 1–16. <https://doi.org/10.1029/2021RS007326>
- Laulainen, J., Kalvas, T., Koivisto, H., Komppula, J., Kronholm, R., & Tarvainen, O. (2016). Photoelectron emission from metal surfaces induced by radiation emitted by a 14 GHz electron cyclotron resonance ion source. *Review of Scientific Instruments*, 87(2), 02A506. <https://doi.org/10.1063/1.4935012>
- Lebreton, J.-P., Stverak, S., Travnicek, P., Maksimovic, M., Klinge, D., Merikallio, S., et al. (2006). The ISL Langmuir probe experiment processing onboard DEMETER: Scientific objectives, description and first results. *Planetary and Space Science*, 54(5), 472–486. <https://doi.org/10.1016/j.pss.2005.10.017>
- Lee, C. K., Han, S. C., Bilitza, D., & Chung, J. K. (2011). Validation of international reference ionosphere models using in situ measurements from GRACE K-band ranging system and CHAMP planar Langmuir probe. *Journal of Geodesy*, 85(12), 921–929. <https://doi.org/10.1007/s00190-011-0442-6>
- Lee, J. C., Min, K. W., Ham, J. W., Kim, H. J., Lee, J. J., & Hong, S. K. (2013). Langmuir probe experiments on Korean satellites. *Current Applied Physics*, 13(5), 846–849. <https://doi.org/10.1016/j.cap.2012.12.011>
- Lee, W.-K., Chun, J.-K., Cho, S.-K., Park, J.-U., Cho, J.-H., Yoon, J.-C., et al. (2007). Retrieval of electron density profile for KOMPSAT-5 GPS radio occultation data processing system. *Journal of Astronomy and Space Sciences*, 24(4), 297–308. <https://doi.org/10.5140/JASS.2007.24.4.297>
- Lomidze, L., Knudsen, D. J., Burchill, J., Kouznetsov, A., & Buchert, S. C. (2018). Calibration and validation of Swarm plasma densities and electron temperatures using ground-based radars and satellite radio occultation measurements. *Radio Science*, 53(1), 15–36. <https://doi.org/10.1002/2017RS006415>
- Marchetti, D., & Akhondzadeh, M. (2018). Analysis of Swarm satellites data showing seismo-ionospheric anomalies around the time of the strong Mexico ($M_w = 8.2$) earthquake of 08 September 2017. *Advances in Space Research*, 62(3), 614–623. <https://doi.org/10.1016/j.asr.2018.04.043>
- Marholm, S., & Marchand, R. (2020). Finite-length effects on cylindrical Langmuir probes. *Physical Review Research*, 2(2), 023016. <https://doi.org/10.1103/PhysRevResearch.2.023016>
- Marklund, G. T., Blomberg, L. G., & Persson, S. (2001). Astrid-2, an advanced microsatellite for auroral research. *Annales Geophysicae*, 19(6), 589–592. <https://doi.org/10.5194/angeo-19-589-2001>
- Marks, M. (2011). Comparing Langmuir probe traces of different Debye length-to-probe radius ratios. *McNair Scholars Research Journal*, 3(1).
- McNamara, L. F., Cooke, D. L., Valladares, C. E., & Reinisch, B. W. (2007). Comparison of CHAMP and digisonde plasma frequencies at jicamarca, Peru. *Radio Science*, 42(2), 1–14. <https://doi.org/10.1029/2006RS003491>
- Morooka, M. W., Wahlund, J. E., Andrews, D. J., Persoon, A. M., Ye, S. Y., Kurth, W. S., et al. (2018). The dusty plasma disk around the Janus/Epimetheus ring. *Journal of Geophysical Research: Space Physics*, 123, 4668–4678. <https://doi.org/10.1002/2017JA024917>
- Noja, M., Stolle, C., Park, J., & Lü, H. (2013). Long-term analysis of ionospheric polar patches based on CHAMP TEC data. *Radio Science*, 48(3), 289–301. <https://doi.org/10.1002/rds.20033>
- Oya, H., Iizima, M., & Morioka, A. (1991). Plasma turbulence disc circulating the equatorial region of the plasmasphere identified by the plasma wave detector (PWS) onboard the Akebono (EXOS-D) satellite. *Geophysical Research Letters*, 18(2), 329–332. <https://doi.org/10.1029/91gl00030>
- Oyama, K. (2015). DC Langmuir probe for measurement of space plasma: A brief review. *Journal of Astronomy and Space Sciences*, 32(3), 167–180. <https://doi.org/10.5140/JASS.2015.32.3.167>
- Oyama, K.-I. (1976). A systematic investigation of several phenomena associated with contaminated Langmuir probes. *Planetary and Space Science*, 24(Issue 2), 183–190. ISSN 0032-0633. [https://doi.org/10.1016/0032-0633\(76\)90104-5](https://doi.org/10.1016/0032-0633(76)90104-5)
- Oyama, K.-I., Lee, C. H., Fang, H. K., & Cheng, C. Z. (2012). Means to remove electrode contamination effect of Langmuir probe measurement in space. *Review of Scientific Instruments*, 83(5), 055113. <https://doi.org/10.1063/1.4722167>
- Park, J., Kwak, Y. S., Mun, J. C., & Min, K. W. (2015). Vertical scale height of the topside ionosphere around the Korean Peninsula: Estimates from ionosondes and the Swarm constellation. *Journal of Astronomy and Space Sciences*, 32(4), 311–315. <https://doi.org/10.5140/JASS.2015.32.4.311>
- Pyo, Y. S., Min, K. W., Choi, Y. W., Lee, D. H., Kang, K. M., Hwang, S. M., et al. (1995). CHARACTERISTICS OF THE CONTAMINATED LANGMUIR PROBE. *Journal of Astronomy and Space Sciences*, 12(2), 234–243.
- Rehman, S., Burchill, J., Eriksson, A., & Marchand, R. (2012). Earth magnetic field effects on Swarm electric field instrument. *Planetary and Space Science*, 73(1), 145–150. <https://doi.org/10.1016/j.pss.2012.10.004>
- Reifman, A., & Dow, W. G. (1949). Dynamic probe measurements in the ionosphere. *Physical Review*, 76(7), 987–988. <https://doi.org/10.1103/physrev.76.987>

- Rochus, P., Defise, J. M., Lecat, J. H., Stockman, Y., Franco, P., Gillis, J. M., et al. (2004). Proba-II payload: A Belgian mini space weather observatory. *International Astronautical Federation - 55th International Astronautical Congress*, 5, 3403–3412. <https://doi.org/10.2514/6.iaac-04-iaa.4.11.2.07>
- Rodríguez-Zuluaga, J., Stolle, C., Yamazaki, Y., Lühr, H., Park, J., Scherliess, L., & Chau, J. L. (2019). On the balance between plasma and magnetic pressure across equatorial plasma depletions. *Journal of Geophysical Research: Space Physics*, 124, 5936–5944. <https://doi.org/10.1029/2019JA026700>
- Rother, M., Schlegel, K., Lühr, H., & Cooke, D. (2010). Validation of CHAMP electron temperature measurements by incoherent scatter radar data. *Radio Science*, 45(6), 1–10. <https://doi.org/10.1029/2010RS004445>
- Ryu, K., Lee, J., Kim, S., Chung, T., Shin, G. H., Cha, W., et al. (2017). Characteristics of the plasma source for ground ionosphere simulation surveyed by disk-type Langmuir probe. *Journal of Astronomy and Space Sciences*, 34(4), 343–351. <https://doi.org/10.5140/JASS.2017.34.4.343>
- Samaniego, J. I., Wang, X., Andersson, L., Malaspina, D., Ergun, R. E., & Horányi, M. (2018). Investigation of coatings for Langmuir probes in an oxygen-rich space environment. *Journal of Geophysical Research: Space Physics*, 123, 6054–6064. <https://doi.org/10.1029/2018JA025563>
- Sarkar, S., Gwal, A. K., & Parrot, M. (2007). Ionospheric variations observed by the DEMETER satellite in the mid-latitude region during strong earthquakes. *Journal of Atmospheric and Solar-Terrestrial Physics*, 69(13), 1524–1540. <https://doi.org/10.1016/j.jastp.2007.06.006>
- Schreiner, W. S., Weiss, J. P., Anthes, R. A., Braun, J., Chu, V., Fong, J., et al. (2020). COSMIC-2 radio occultation constellation: First results. *Geophysical Research Letters*, 47(4), 1–7. <https://doi.org/10.1029/2019GL086841>
- Schreiter, L., Montenbruck, O., Zangerl, F., Siemes, C., Arnold, D., & Jäggi, A. (2021). Bandwidth correction of Swarm GPS carrier phase observations for improved orbit and gravity field determination. *GPS Solutions*, 25(2), 1–13. <https://doi.org/10.1007/s10291-021-01107-0>
- Shinbori, A., Ono, T., Iizima, M., Kumamoto, A., Shirai, S., Hanaoka, A., et al. (2007). Electrostatic electron cyclotron harmonic waves observed by the Akebono satellite near the equatorial region of the plasmasphere. *Earth Planets and Space*, 59(6), 613–629. <https://doi.org/10.1186/bf03352723>
- Singh, A. K., Maltseva, O., & Panda, S. K. (2021). Comparison between Swarm measured and IRI-2016, IRI-Plas 2017 modeled electron density over low and mid latitude region. *Acta Astronautica*, 189(September), 476–482. <https://doi.org/10.1016/j.actastro.2021.09.017>
- Smirnov, A., Shprits, Y., Zhelavskaya, I., Lühr, H., Xiong, C., Goss, A., et al. (2021). Intercalibration of the plasma density measurements in Earth's topside ionosphere. *Journal of Geophysical Research: Space Physics*, 126, e2021JA029334. <https://doi.org/10.1029/2021JA029334>
- Su, F., Wang, W., Burns, A. G., Yue, X., & Zhu, F. (2015). The correlation between electron temperature and density in the topside ionosphere during 2006–2009. *Journal of Geophysical Research: Space Physics*, 120, 10724–10739. <https://doi.org/10.1002/2015JA021303>
- Szuszczewicz, E. P., & Holmes, J. C. (1975). Surface contamination of active electrodes in plasmas: Distortion of conventional Langmuir probe measurements. *Journal of Applied Physics*, 46(12), 5134–5139. <https://doi.org/10.1063/1.321572>
- Takahashi, T., Oya, H., & Yamagishi, H. (1981). *Observations of electron density in the polar ionosphere using the swept frequency impedance probe*. National Institute Polar Research Memoirs.
- Wang, X., Malaspina, D. M., Hsu, H.-W., Ergun, R. E., & Horányi, M. (2014). The effects of magnetic fields on photoelectron-mediated spacecraft potential fluctuations. *Journal of Geophysical Research: Space Physics*, 119, 7319–7326. <https://doi.org/10.1002/2014JA019923>
- Winkler, C., Strele, D., Tscholl, S., & Schrittwieser, R. (2000). On the contamination of Langmuir probe surfaces in a potassium plasma. *Plasma Physics and Controlled Fusion*, 42(2), 217–223. <https://doi.org/10.1088/0741-3335/42/2/311>
- Xiong, C., Lühr, H., & Ma, S. Y. (2013). The magnitude and inter-hemispheric asymmetry of equatorial ionization anomaly-based on CHAMP and GRACE observations. *Journal of Atmospheric and Solar-Terrestrial Physics*, 105–106, 160–169. <https://doi.org/10.1016/j.jastp.2013.09.010>
- Yan, R., Guan, Y., Miao, Y., Zhima, Z., Xiong, C., Zhu, X., et al. (2022). The regular features recorded by the Langmuir probe onboard the low Earth polar orbit satellite CSES. *Journal of Geophysical Research: Space Physics*, 127, e2021JA029289. <https://doi.org/10.1029/2021JA029289>
- Yang, T., Park, J., Kwak, Y., Oyama, K., Minow, J. I., & Lee, J. (2020). Morning overshoot of electron temperature as observed by the Swarm constellation and the international space station. *Journal of Geophysical Research: Space Physics*, 125, 1–13. <https://doi.org/10.1029/2019ja027299>
- Yue, X., Schreiner, W. S., Pedatella, N., Anthes, R. A., Mannucci, A. J., Straus, P. R., & Liu, J. Y. (2014). Space weather observations by GNSS radio occultation: From FORMOSAT-3/COSMIC to FORMOSAT-7/COSMIC-2. *Space Weather*, 12(11), 616–621. <https://doi.org/10.1002/2014SW001133>
- Zakharenkova, I., Cherniak, I., & Krankowski, A. (2019). Features of storm-induced ionospheric irregularities from ground-based and spaceborne GPS observations during the 2015 St. Patrick's day storm. *Journal of Geophysical Research: Space Physics*, 124, 10728–10748. <https://doi.org/10.1029/2019JA026782>